

Structure of Polymeric Carbon Dioxide CO₂-V

Frédéric Datchi,¹ Bidyut Mallick,¹ Ashkan Salamat,² and Sandra Ninet¹

¹IMPMC, UPMC/Paris 6, CNRS, 4 place Jussieu, F-75252 Paris Cedex 05, France

²European Radiation Synchrotron Facility, F-38043 Grenoble Cedex, France

(Received 2 November 2011; published 19 March 2012)

The structure of polymeric carbon dioxide (CO₂-V) has been solved using synchrotron x-ray powder diffraction, and its evolution followed from 8 to 65 GPa. We compare the experimental results obtained for a 100% CO₂ sample and a 1 mol % CO₂/He sample. The latter allows us to produce the polymer in a pure form and study its compressibility under hydrostatic conditions. The high quality of the x-ray data enables us to solve the structure directly from experiments. The latter is isomorphic to the β -cristobalite phase of SiO₂ with the space group $I\bar{4}2d$. Carbon and oxygen atoms are arranged in CO₄ tetrahedral units linked by oxygen atoms at the corners. The bulk modulus determined under hydrostatic conditions, $B_0 = 136(10)$ GPa, is much smaller than previously reported. The comparison of our experimental findings with theoretical calculations performed in the present and previous studies shows that density functional theory very well describes polymeric CO₂.

DOI: 10.1103/PhysRevLett.108.125701

PACS numbers: 64.70.km, 61.50.Ks, 62.50.-p, 64.30.Jk

The discovery of a crystalline, polymeric form of carbon dioxide (CO₂-V) when the latter is submitted to high pressures ($P \sim 40$ GPa) and temperatures ($T \sim 1800$ K) [1] has revealed the existence of a new class of CO₂ solids with properties very different from the previously known molecular forms. This material has attracted a lot of interest as it was reported to have large nonlinear optical coefficients and a very high bulk modulus of 365 GPa, comparable to the superhard cubic BN [2], and thus could have important applications if available at ambient conditions. Iota *et al.* [1] could quench CO₂-V down to 1 GPa at 300 K, which is very far from the thermodynamic conditions of its synthesis, but it reverted to a molecular form at lower pressures. Understanding the properties of polymeric CO₂ also has important implications for the chemistry of deep Earth, as recent studies indicate that it could be largely present in the lower mantle [3–6].

A central, yet unsettled question relates to the structure of this material. Obtaining high-quality structural data at the extreme conditions of formation of phase V is indeed experimentally challenging, which may explain why there are so few experimental studies reported to date [2,7]. This is in contrast with the several theoretical investigations devoted to this issue [5,8–12]. Yoo *et al.* measured the x-ray diffraction (XRD) pattern of a temperature-quenched CO₂-V sample at 48 GPa and 300 K [2], produced by indirectly heating CO₂ via laser irradiated ruby pieces. Although the data quality did not allow the authors to solve nor refine the structure, they proposed a $P2_12_12_1$ model similar to the tridymite structures of SiO₂, composed of interconnected layers of CO₄ tetrahedral units. This structure and several other isomorphs of SiO₂ have been investigated using density functional theory (DFT). Serra *et al.* first predicted the α -quartz structure as the most stable above 35 GPa [8]. Dong *et al.* [9,10] compared several

candidates and found that the tetragonal β -cristobalite structure with space group $I\bar{4}2d$ had the lowest enthalpy. Moreover, they observed that the experimental $P2_12_12_1$ structure proposed in Ref. [2] was far from equilibrium. Holm *et al.* [11] agreed that the β -cristobalite form has the lowest enthalpy at 0 K but argued that the $P2_12_12_1$ structure could be stabilized at the high temperature conditions of the experiment. More recently, evolutionary structure searches by Oganov *et al.* [5] supported the stability of β cristobalite at pressures 50–150 GPa and 0 K, but also suggested some new competitive metastable forms. Using metadynamics calculations [12], or by analyzing possible transition pathways [13], it was found that, despite its higher enthalpy, the $P4_12_12$ α -cristobalite structure may be easier to form in the stability range of phase V. Very recently, Seto *et al.* [7] measured the x-ray pattern of CO₂-V samples produced by direct CO₂-laser heating at pressures of 40–90 GPa. Their patterns are different from those of Ref. [2] and agreed qualitatively with that of the β -cristobalite structure. However, the quality of their data was again not sufficient to solve nor refine the structure.

In this Letter we report the solution of the structure of CO₂-V based on new synchrotron XRD data. We succeeded in obtaining high-quality powders of *pure* CO₂-V thanks to an original sample topology making use of the properties of CO₂-helium mixtures. Our results show that CO₂-V is indeed isomorphous to β cristobalite with space group $I\bar{4}2d$, and that its compressibility is well described by DFT.

To achieve the high pressures and temperatures needed to produce CO₂-V, we used the laser-heated diamond anvil cell technique [14]. There are two well-known issues regarding this technique. First, chemical reactions may occur between the sample and the materials used to couple with the infrared laser or those used to thermally insulate the

sample from the diamond anvils. Even stable and chemically inert materials at ambient conditions may easily react at high P - T , as is the case, for example, for N_2 with platinum [15]. Second, laser heating produces large temperature gradients inside the sample, especially when the latter is not thermally insulated from the diamond anvils. In the case of CO_2 , this results in an incomplete transformation of the sample into the polymeric phase, and its mixing with other molecular phases (III, II, and/or IV) which are all metastable at room temperature. This is especially problematic for structural determination as it makes indexing of Bragg reflections ambiguous.

In order to overcome these problems, we make use of our recent investigation of the CO_2/He binary diagram at 295 K, which shows that the two components are completely separated above the solidification pressure of He, whatever the initial concentration [16,17]. By loading a CO_2/He mixture, it is thus possible to grow a pure sample of solid CO_2 embedded in helium in the sample chamber of a diamond anvil cell. Helium provides a thermal insulating layer between the CO_2 sample and the diamond anvils, as well as a quasihydrostatic pressure medium. Furthermore, we used a CO_2 laser ($\lambda = 10.6 \mu m$) to directly heat the CO_2 sample, as in Refs. [7,18], to prevent any potential reaction between CO_2 and a laser absorbing material.

We performed measurements on both a 100% CO_2 sample and a 1 mol % CO_2/He sample to allow for comparison (see Experimental methods in Ref. [17]). The large concentration of He in the mixed sample was chosen to ensure that the CO_2 component was completely surrounded by He. The 100% CO_2 sample was first laser heated at 21 GPa up to ~ 1800 K, which produced a mixture of molecular phases II and IV. It was then compressed to 39 GPa and laser heated again to ~ 1800 K to obtain phase V [2]. The CO_2/He sample was directly compressed to 44 GPa at 295 K, where it was in molecular phase III, and then laser heated to ~ 1800 K. As seen in Fig. 1, the Raman spectra measured at 295 K from the laser-heated CO_2/He sample displays the characteristic peaks of CO_2 -V [1,19] (see also Ref. [17]) and no signature of molecular CO_2 , showing that the transformation was complete. By contrast, the Raman spectra of the 100% CO_2 sample displayed modes from both CO_2 -V and unreacted molecular CO_2 . The fact that CO_2 -V is obtained by annealing different molecular phases or mixture of phases is consistent with previous reports [1,19].

The x-ray images collected at 295 K from the two samples showed in both cases full powder rings indicative of high-quality powders [17]. Integration of these images produces the spectra shown in Fig. 1. For the CO_2/He sample, we readily identified the Bragg peaks from He and the Re gasket using the known structures and equations of state of these two elements. Comparison of the set of remaining peaks with the spectrum of the 100% CO_2 sample allowed us to identify the peaks from CO_2 -V in the

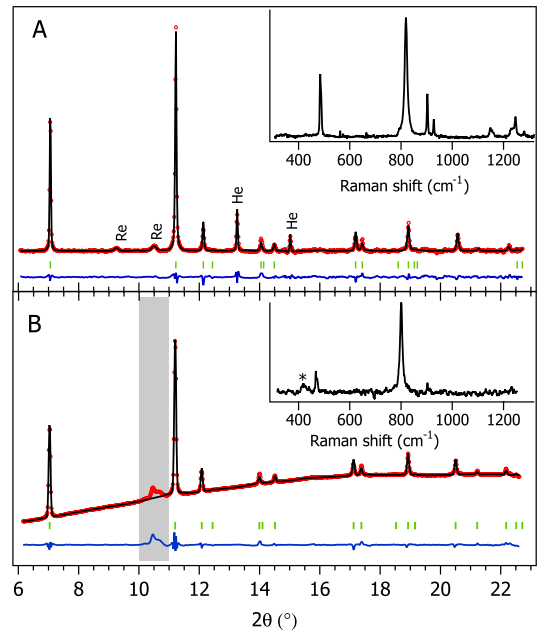


FIG. 1 (color online). XRD patterns collected at 41 GPa and 295 K after laser heating: (a) $CO_2(1\%)/He$ sample and (b) 100% CO_2 sample. The x-ray wavelength was 0.3738 \AA . Red circles, experimental data; black lines, full profile refinements; gray (blue) lines, fit residuals; green sticks, positions of diffraction lines. In (a), the background has been subtracted for easier visualization and diffraction lines from the He component and Re gasket are indicated. In (b), the grayed region has been excluded from refinement as it contains only reflections from untransformed molecular CO_2 . The insets show the respective Raman spectra collected from the same samples at 48 GPa (a) and 41 GPa (b). The * symbol indicates modes from unreacted molecular CO_2 . The weak modes of CO_2 -V are more difficult to observe in (b) due to a larger luminescence background from the diamond anvils.

latter spectrum. In particular, the small peaks observable at $10^\circ < 2\theta < 11^\circ$ in Fig. 1(b) do not appear in Fig. 1(a) and thus come from untransformed molecular CO_2 .

Indexing of the 11 observed peaks between 7° and 22.2° strongly suggested a tetragonal unit cell with lattice parameters $a = b = 3.552(2) \text{ \AA}$ and $c = 5.919(3) \text{ \AA}$ at 41 GPa (numbers in parentheses represent uncertainties at 3σ level). To estimate the number Z of CO_2 per unit cell in the polymer, we compared its volume (V_V) to that of the molecular phase III (V_{III}) at the same pressure, measured in the same experiment. For Z equal to 3, 4, and 5, the relative difference in volume $[(V_V - V_{III})/V_{III}]$ at 41 GPa is, respectively, $+7.4\%$, -19.5% , and -35.6% . Clearly $Z = 3$ is impossible, whereas the volume reduction for $Z = 4$ is very similar to that found in N_2 at the molecular-polymeric transition (-22%) [20], and seems the more likely.

Based on the systematic absences of Bragg reflections, the most probable space groups are $I4_1/amd$, $I4_1/md$, and $I\bar{4}2d$. Structure solution was thus sought for each of these

space groups and for $Z = 4$ or 5 , using the direct-space method implemented in the ENDEAVOUR software (Crystal Impact) [21]. No physically reasonable solution was found for $I4_1/amd$ and $I4_1md$, while the search rapidly converged for $I\bar{4}2d$ and $Z = 4$ to a solution with a low Bragg R factor of 9%. As a matter of fact, starting with space group $P1$ and $Z = 4$, the search also invariably converged to the same $I\bar{4}2d$ structure, showing that it is a deep minimum of the cost function. Full profile refinements of the XRD patterns using FULLPROF [22] produced final Bragg R factors of 3.6% and 3.1% for the 100% CO_2 and CO_2/He samples, respectively (more details in Ref. [17]).

The structure of $\text{CO}_2\text{-V}$ is displayed in Fig. 2(a). The asymmetric unit is composed of one C atom at $(0, 0, 0)$ and one O atom at $(x, 0.25, 0.125)$, with $x = 0.214(2)$ at 41 GPa. The structure may be described as a network of CO_4 tetrahedra bridged by oxygen atoms at the corners. The C-O distance is the same for all pairs within the

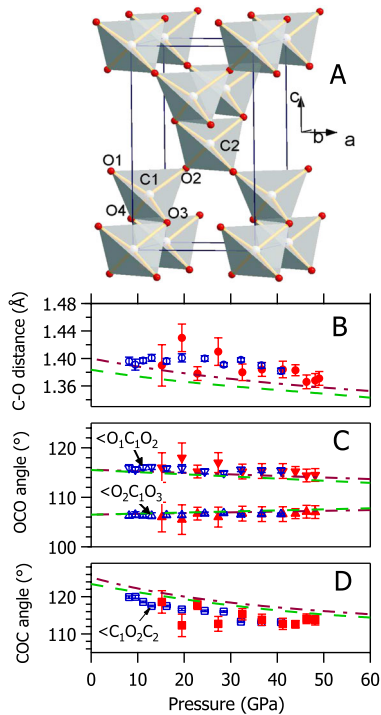


FIG. 2 (color online). (a) Unit cell of polymeric carbon dioxide phase V: C atoms in white and O atoms in gray (red). The CO_4 tetrahedral units are emphasized with gray polyhedra. (b)–(d) Evolution with pressure of the C-O bond distance, intratetrahedral, and intertetrahedral angles, respectively. Hollow and solid symbols represent experimental data from the 100% CO_2 sample and the 1 mol % CO_2/He sample, respectively; error bars come from statistical analysis of profile refinements [22], evaluated at the 3σ level. The larger uncertainties for the CO_2/He sample are mostly due to the small content of CO_2 which resulted in weaker signals [17]. Dashed lines and dash-dotted lines are from DFT calculations with LDA or GGA approximations, respectively.

tetrahedra, taking the value of $1.38(1)$ Å at 41 GPa, but there are two different intratetrahedral $\angle\text{OCO}$ angles of $106.6(2)^\circ$ and $115.4(5)^\circ$. The angle of the C-O-C bridge between two tetrahedra is $113.2(2)^\circ$. This structure is iso-morphous to the β -cristobalite phase of SiO_2 and is also common to other AB_2 compounds such as ZnCl_2 and GeSe_2 . This is also the structure which was predicted as the most stable in most DFT studies [5,9–12].

X-ray patterns from the two samples were further collected at 295 K on decompression from 48 to 8 GPa. An additional data point was obtained at 65 GPa on a third sample composed of a 5 mol % CO_2/He mixture, but the quality of the x-ray pattern only allowed us to extract the lattice parameters in this case. Phase V could be observed down to 8 GPa, where the back transformation to molecular phase I started and completed at 6 GPa. For the 100% CO_2 sample, the x-ray patterns collected between 30 and 15 GPa showed broadened diffraction lines, and their refinements were of poorer quality, whereas the mixed CO_2/He sample presented very sharp diffraction lines over the whole pressure range [17]. We interpret this broadening as due to some nonhydrostatic strain developing in the 100% CO_2 sample, since no pressure transmitting medium is present in this case. As we will see below, this results in a different equation of state in the range 15–30 GPa between the two samples; however, the internal parameters of the $\text{CO}_2\text{-V}$ structure determined from either sample agree within error bars.

As can be observed from Figs. 2(b) and 2(c), the C-O distance and intratetrahedral $\angle\text{OCO}$ angles of the $\text{CO}_2\text{-V}$ structure are barely affected by pressure between 8 and 50 GPa: the C-O distance slightly decreases by 2% and the two angles change by less than 1° . The shape of the CO_4 tetrahedral unit thus barely changes in this pressure range. Similarly, the small dependence on pressure of the intertetrahedral $\angle\text{COC}$ angle evidences the rigidity of the C-O-C bridge, as previously noted by Dong *et al.* from calculations [10]. We compare our measurements to our own DFT calculations, using either the local-density approximation (LDA) or the generalized-gradient approximations (GGA) [23] (see Theoretical methods in Ref. [17]). Figure 2 shows the excellent agreement between DFT and experiments; there is little difference between the LDA and GGA results, although the C-O distance is better described by GGA.

The variations with pressure of the lattice parameters and volume of $\text{CO}_2\text{-V}$ are presented in Fig. 3. There is good agreement between the data of the two samples, except in the 15–30 GPa pressure range where nonhydrostatic effects were observed in the 100% CO_2 sample. This shows clearly on the length of the c axis: while it exhibits a maximum around 25 GPa in the 100% sample, it shows a shallow minimum at about the same pressure in the hydrostatically compressed sample, in much better correspondence with DFT. Similar observations can be made for the volume,

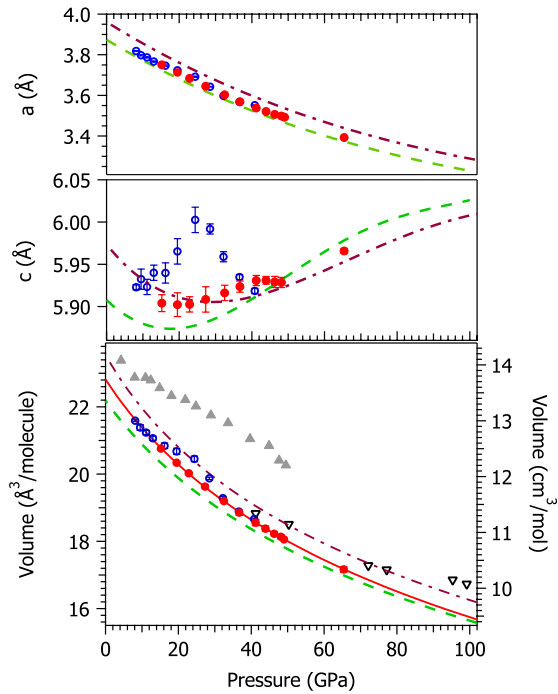


FIG. 3 (color online). Lattice parameters and volume of $\text{CO}_2\text{-V}$ as a function of pressure. Hollow and solid circles are present experimental data from the 100% CO_2 sample and the $\text{CO}_2(1\%)/\text{He}$ sample, respectively; the solid line is the Birch-Murnaghan fit to the CO_2/He sample data. Dashed lines and dash-dotted lines represent DFT calculations using the LDA and GGA approximations, respectively. Up-pointing triangles and down-pointing triangles are measurements from Refs. [2,7], respectively.

which presents an anomalous variation in the 100% sample between 15 and 30 GPa, but not in the CO_2/He mixed one. To extract the compressibility of $\text{CO}_2\text{-V}$, we thus only use the data from the CO_2/He sample. The zero-pressure volume V_0 , bulk modulus B_0 , and its pressure derivative B'_0 obtained from a fit to the Birch-Murnaghan equation of state are $V_0 = 13.7(1) \text{ cm}^3/\text{mol}$, $B_0 = 136(11) \text{ GPa}$, and $B'_0 = 3.7(4)$. This is very close to what is obtained from our DFT calculations [$B_0 = 144(2) \text{ GPa}$, $B'_0 = 3.95(5)$ for LDA, $B_0 = 135(1) \text{ GPa}$ and $B'_0 = 3.82(2)$ for GGA], which themselves agree well with previous reports [5,10]. Our experimental value of B_0 is much lower than that reported by Ref. [2] (365 GPa), thus questioning the superhard nature of $\text{CO}_2\text{-V}$. The β -cristobalite phase of CO_2 is, however, much more rigid than the one of SiO_2 ($B_0 \sim 22 \text{ GPa}$ [24]), a fact which can be linked to the lower flexibility of the C-O-C bridge in comparison to the Si-O-Si one [5,10].

Why the XRD patterns of $\text{CO}_2\text{-V}$ reported in Ref. [2] are different from those obtained here and in Ref. [7] is not clear at present, but could be due to a chemical reaction between CO_2 and ruby since Yoo *et al.* [2] used ruby to absorb the YAG laser in their experiments. Indeed,

Seto *et al.* reported that CO_2 can easily react with Al_2O_3 at high P - T [7]. Figure 3 also shows that the volumes reported for phase V in Ref. [2] are $\sim 12\%$ larger than present ones. Though closer, the volumes of Ref. [7] are also consistently larger than ours, which is likely due to the different means of measuring pressure in the two experiments [25].

In conclusion, we have reported here clear experimental evidence that polymeric $\text{CO}_2\text{-V}$ adopts the $I42d$ β -cristobalite structure, and is more compressible than previously claimed [2]. Our experimental results are well in line with most published DFT predictions. Besides solving a long-standing question, the knowledge of the $\text{CO}_2\text{-V}$ structure may now be confidently used to investigate the properties of this interesting compound, its stability with respect to other CO_2 polymorphs, and its chemical reactivity with other materials, such as, for example, minerals inside Earth's mantle.

We acknowledge the ESRF for provision of beam time under proposal HS4211, M. Mezouar, G. Garborino, and P. Bouvier for their help on ID27 beam line, and G. Rousse (IMPIC) for her help with FULLPROF. Calculations were performed at the IDRIS supercomputing center under Project No. 090208.

-
- [1] V. Iota, C.S. Yoo, and H. Cynn, *Science* **283**, 1510 (1999).
 - [2] C.S. Yoo, H. Cynn, F. Gygi, G. Galli, V. Iota, M. Nicol, S. Carlson, D. Häusermann, and C. Mailhot, *Phys. Rev. Lett.* **83**, 5527 (1999).
 - [3] N. Takafuji, K. Fujino, T. Nagai, Y. Seto, and D. Hamane, *Phys. Chem. Miner.* **33**, 651 (2006).
 - [4] Y. Seto, D. Hamane, T. Nagai, and K. Fujino, *Phys. Chem. Miner.* **35**, 223 (2008).
 - [5] A. R. Oganov, S. Ono, Y. Ma, C. W. Glass, and A. Garcia, *Earth Planet. Sci. Lett.* **273**, 38 (2008).
 - [6] K.D. Litasov, A. Goncharov, and R.J. Hemley, *Earth Planet. Sci. Lett.* **309**, 318 (2011).
 - [7] Y. Seto, D. Nishio-Hamane, T. Nagai, N. Sata, and K. Fujino, *J. Phys. Conf. Ser.* **215**, 012015 (2010).
 - [8] S. Serra, C. Cavazzoni, G.L. Chiarotti, S. Scandolo, and E. Tosatti, *Science* **284**, 788 (1999).
 - [9] J. Dong, J. K. Tomfohr, and O. F. Sankey, *Phys. Rev. B* **61**, 5967 (2000).
 - [10] J. Dong, J. K. Tomfohr, O. F. Sankey, K. Leinenweber, M. Somayazulu, and P. F. McMillan, *Phys. Rev. B* **62**, 14685 (2000).
 - [11] B. Holm, R. Ahuja, A. Belonoshko, and B. Johansson, *Phys. Rev. Lett.* **85**, 1258 (2000).
 - [12] J. Sun, D. D. Klug, R. Martoňák, J. A. Montoya, M.-S. Lee, S. Scandolo, and E. Tosatti, *Proc. Natl. Acad. Sci. U.S.A.* **106**, 6077 (2009).
 - [13] A. Togo, F. Oba, and I. Tanaka, *Phys. Rev. B* **77**, 184101 (2008).
 - [14] M. Eremets, *High-Pressure Experimental Methods* (Oxford University Press, New York, 1996).

- [15] E. Gregoryanz, C. Sanloup, M. Somayazulu, J. Badro, G. Fiquet, H. K. Mao, and R. Hemley, *Nature Mater.* **3**, 294 (2004).
- [16] B. Mallick, F. Datchi, and S. Ninet (to be published).
- [17] See Supplemental Material at <http://link.aps.org/supplemental/10.1103/PhysRevLett.108.125701> for more information on experimental and theoretical methods, XRD and Raman data.
- [18] O. Tschauer, H. K. Mao, and R. J. Hemley, *Phys. Rev. Lett.* **87**, 075701 (2001).
- [19] M. Santoro, J. F. Lin, H. K. Mao, and R. J. Hemley, *J. Chem. Phys.* **121**, 2780 (2004).
- [20] M. Eremets, A. G. Gavriluk, N. R. Serebryanaya, I. A. Trojan, D. A. Dzivenko, R. Boehler, H. K. Mao, and R. J. Hemley, *J. Chem. Phys.* **121**, 11296 (2004).
- [21] H. Putz, J. C. Schön, and M. Jansen, *J. Appl. Crystallogr.* **32**, 864 (1999).
- [22] J. Rodriguez-Carvajal, *Physica (Amsterdam)* **192B**, 55 (1993); see <http://www.ill.eu/sites/fullprof/>.
- [23] J. P. Perdew, K. Burke, and M. Ernzerhof, *Phys. Rev. Lett.* **77**, 3865 (1996).
- [24] T. Demuth, Y. Jeanvoine, J. Hafner, and J. Ángyán, *J. Phys. Condens. Matter* **11**, 3833 (1999).
- [25] Reference [7] used the Raman mode of the diamond anvil, which is known to be less accurate than the well-calibrated SrB₄O₇:Sm²⁺ fluorescence sensor used in the present case.